Materials Science Forum
ISSN: 1662-9752, Vol. 1050, pp 51-63

Submitted: 2021-05-16
Revised: 2021-08-11
Accepted: 2021-08-11
Online: 2022-01-18

Plasma Jet Prepared Gold and Silver Nanoparticles to Induce Caspase-Independent Apoptosis in Digestive System Cancers

Mohammed Subhi Mohammed[1,a], Ban H.Adil[2,b] ,A.S. Obaid[3,c], Ahmed Majeed Al-Shammari[4,d]

[1]Community health department, Kufa Technical Institute, Al-Furat Al-Awsat Technical University. Iraq

[2]University of Baghdad, College of Science for Women, Baghdad, IRAQ

[3]Department of Physics, College of Science, University of Anbar, Ramadi, Iraq

[4]Expermental Therapy Department, Iraqi Center for cancer and Medical Genetics Research, Al-Mustansiriyah University, Baghdad, IRAQ

[a]mohammed.mohammed@atu.edu.iq, [b]banha_phys@csw.uobaghdad.edu.iq, [c]ahmed.sobaid.alqayssei@gmail.com, [d]Ahmed.alshammari@iccmgr.org

Keywords: Ag NPs, Au NPs, cold plasma, Gene expression, cytotoxicity, HC cell line, SK-GT-4 cell line, REF cell line

Abstract. Alot of medical and industrial applications used the metal nanoparticles (NPs) with increase interest to be used as cancer therapy. The current work aimed to prepare AuNPs and AgNPs through the use of plasma jet and test their antitumor mechanism of apoptosis induction. The results indicating the face-centered cubic structures and crystalline nature of AuNPs and AgNPs. Also, the image of FESEM showed that the well dispersions regarding AuNPs and AgNPs, while the NP's spherical shape with the particle size distributions which are considered to be close that estimated from the XRD. cytotoxicity have been assessed against the Normal embryonic cell line REF and the digestive system (HC , SK-GT-4) cell lines under a variety of the series dilute of the Ag and Au NPs (6.25, 12.5, 25, 50 and 100%), have been determined through a microtetrazolium (MTT) assay. The capacity of Ag and Au NPs to induce apoptosis to an infected cell has been studied by crystal violet stain to measure the percentage of induction of apoptosis. In cases where 100 µg\ml Au NP concentrations are 69.60 percent, the maximum cytotoxicity of the HC cell line was reported, while 100 µg\ml Au NP was 69.20% for the SKg cell line exposure. qRT-PCR in AuNPs and AgNPs treated of (HC and SKG) cell lines revealed a remarkable in the expression of BAX, BCL2 and AIF, Endo G (independent pathway).

Background

The nano-science along with its approaches has been defined as interdisciplinary sciences of high importance in various fields due to the fact that their surface area is high, optimum comparative properties with low-density, high surface interaction as well as various approaches [1]. Thanks to their distinctive physical characteristics, metal particles with a size in (nanometres) have been of high importance lately. New applications are provided due to the fact that their electrical and optical properties are different from the others [2]. The major significant nano-sized metals are AgNPs and AuNPs, which are utilized in various applications [3]. Different approaches applied for obtaining particles with the needed properties. Thus, the particle's distribution, shape, or size are essential [4]. A lot of techniques are utilized to conserve the fixed properties regarding NPs solutions (chemical surface treatment, polymer stability, and electrostatic force stabilization) [5]. In addition, the processes might be categorized into dispersants as well as condensations to process the colloidal NP solutions. In addition, the atmospheric pressure plasma can be defined as a plasma that is non-balance (or non-thermal) since the temperature of electron is high in comparison to the ions' temperature [6]. AgNPs and AuNPs were utilized in targeted drug-delivery, cell structure's visualization, bio-sensor researches, and nanobiotechnology [7]. Currently, the colloidal NPs are examined due to their distinctive physicochemical characteristics differing from those related to 'bulk'[8]. The size and form

of NPs are of high importance in all nanotechnology applications. The distinctive properties of the metal NPs inducing their applications, like environment's protection and fuel cells, the nano-clusters might be prepared on periodic pattern surfaces for the sensor's enhancement, such applications have distinctive optical properties since their major principle of operation, especially Localized Surface Plasmon Resonance, which can be abbreviated to (LSPR)[9, 10].
Conflicting results might be presented due to the differences in cell lines, physical and chemical properties, and toxicity tests of NPs. However, there is a common agreement that toxicity is the result of being exposed to AgNPs in different normal cell lines and cancer lines [11]. Furthermore, the cytotoxic impact approach proposed via AuNPs and AgNPs, production of induction related to Reactive Oxygen Species (ROS) verified via researches indicated that the decrease in glutathione high ROS contents as well as the lipid peroxidation because of the in-vitro exposures to the nanoparticles [12-14].
The increase in ROS that is moderated through AuNPs and AgNPs have been apoptosis and DNA damage, which were related [15]. The apoptosis can be defined as one of the selective mechanisms regulating the balances between the cell's death and cell proliferation in the physiological cells. [16]. In addition, many stimuli of the cellular stress were indicated, such as oxidative stress, μ radiation, chemical therapeutics, trophic factor, absence of the growth factor, irradiation, death receptor activations, glucocorticoids, DNA as well as endoplasmic reticulum because of endoplasm were triggering apoptosis. The exposure of cells to certain conditions including the absence of oxygen, protein glycosylation inhibition, serum and glucose hunger, as well as the homeostasis disorder regarding Ca2 + [17]. The apoptosis occurs as an approach of defence, in which the cells were additionally weakened, the repair capacity, especially in the case when damage resulting from toxicants or disease is impacting the cellular DNA, also the mechanisms of cell repair might not be fixing the damages [18]. The cell's death can be identified through various morphological alterations, like nuclear condensation, blebbing, in addition to disorder and genomic DNA fragmentations. [18] Furthermore, the apoptosis was indicated as a significant approach for AuNPs and AgNPs-toxicity resulting from various cell types and animals cultivated [19, 20].
The mitochondria are considered essential to cell death regulations. A lot of the damage pathways and pro-apoptotic factors are contributing to mitochondrial release regarding apoptogenic signaling molecules, for instance, Endo-G, AIF, procaspases, and cyt c (one might refer to the mitochondrial opening regarding mitochondry cause oxidative stress), also the overproduction of ROS [21]. Gold and silver-induced apoptosis can be defined as the major activation of the apoptosis of the mitochondria. [22]. A lot of researches was focusing on AIF/EndoG caspases-independent apoptotic pathways. In addition, BNIP3 (Bcl2/Adenovirus E1B 19kDa interacting protein-3) triggering the caspase-independent apoptosis which is inducing the AIF's mitochondrial release; EndoG function as modulator [23].
The present work aims to determine the involvement of caspase-independent apoptotic pathway induced by AuNPs and AgNPs.

Methods

Preparation of the solution

In this study, the ($HAuCl_4.4\ H_2O$) aqueous tetra-chloride salts have been utilized (99% purity and 411.8476 g /mol partial weight) created via SGMA (Germany). 2 mL of 0.40mM, AgNO3 (169.872 g/mol as partial weight) have been prepared, the next equation (1) is applied for calculating the needed weight:

$$\text{Concentration (mole)} = (\text{mass (g)}) / (\text{Molecular weight (g / mol)} \times \text{volume (liter)}) \ldots \quad (1)$$

Preparation of nanoparticles

The next steps are conducted to prepare the AuNPs:
Vertically, the catcher is used to fix the metal tube for a diameter of 1 mm, following preparing the solution of salts related to silver and gold with the needed sizes and concentrations, the prepared form

will be put on holder within the metal tube as indicated in details. In addition, the beaker was rounded from metals tube to a distance between liquid surface as well as tube's nozzle has been 1mm. Furthermore, Argon gas that is provided in metal tube was regulated via Sanpur gas flow controlled. There was a gradual increase in the value related to the system's supplied voltage until the plasms were created between the liquid's surface and the tube as can be seen in figure (1)

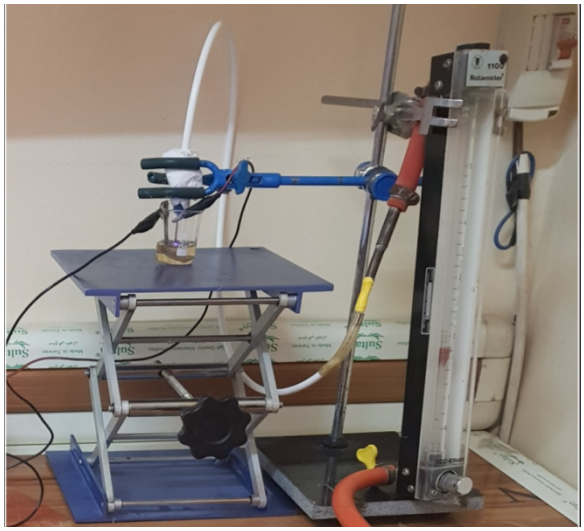

Figure 1. Illustrates the cold plasma system generating nanomaterials

Cytotoxicity Assay

Hepato cancer cell lines (HCAM) as well as the oesophagus adenocarcinoma cell lines (SK-GT-4) were acquired from the Department of Experimental Therapy, Iraqi Centre for Cancer, and Medical Genetic Research (ICCMGR; Baghdad, Iraq). This study used the normal cell lines and cancer cell lines. With regard to tissue culture, the study used a microtiter plate of 96 (12×8), each one of the cells utilized for seeding 10,000 cells, for being incubated for a period of 25hrs at a temperature of 37^{o}C, till the monolayer has been achieved as indicated via the inverted microscope. In addition, the cells are subjected to series dilute AgNPs and AuNPs, while the control wells have been left with no treatment. The already-indicated steps have been achieved in triplicate, after that subjected to re-incubation at a temperature of 37oC. Following incubation for 48 hours, the growth medium has been decanted-off, the steps have been done 3 times for confirming the veracity. Furthermore, the MTT of (100µL that is diluted through free serum medium of 1mL) has been added (MMT dilute of 100µL for each one of the wells) prior to it being subjected to incubation for a period of 2hrs, after that decanted-off, then DMSO is added (50µL for each one of the wells) and subjected to re-incubation at a temperature of 37 Celsius for a period of 40mins. Also, the microplate reader has been applied for reading the results at wavelengths of 584 for calculating the percentage regarding live cancer cells (inhibition rate), after that the mean value will be estimated for each one of the groups. With the use of crystal violet, the cells have been examined within an inverted microscope as well as being photographed via digital camera and separately recorded for the results. GraphPad Prism v7.0 is used to analyze the experimental results **[24-26]**

Samples for RT-PCR:

The flakes (25cm2) which ar related to tissue culture which contain 1^{6}cells/flask were subjected to incubation at a temperature of 37 Celsius for a period of 24hrs. The medium was removed from flasks, while the gold and silver were inoculated. Also, the negative control was just treated for the use of free serum medium. [27]. Every one of the flasks has been re-incubated at a temperature of 37 Celsius for 48hrs.

Table 1. Sequence of primersSynthesis of silver nanoparticles and gold nanoparticles Characterization of colloidal silver and gold nanoparticles

NO	primers	F\R	Sequence '5 - … - '3
1	BAX	F	GTTTGCCCTCGGATCTCTGG
		R	GCTTCCAACAGCGTAAATCCAA
2	BCL2	F	GGTGGGGTCATGTGTGTGG
		R	CGGTTCAGGTACTCAGTCATCC
3	AIF Apoptosis inducing factor	F	GGGAGGACTACGGCAAAGGT
		R	CTTCCTTGCTATTGGCATTCG
4	Endo G Endonuclease G	F	CTCATCACCTAGTTCCTTGG
		R	GGAAGCATGTGACATCAACC
5	GAPDH Housekeeping gene	F	CTGGGCTACACTGAGCACC
		R	AAGTGGTCGTTGAGGGCAATG

RNA"extraction:

Negative and infected control cells which are harvested at 48 with use of full-RNA extraction kit (AccuZol ^{TM}) obtained the Total RNA. Also, the nano-drop has been applied for detecting the RNA concentrates in the ng / μL as well as the purity through estimating the optical density ratio at (260/280nm) through wave-length of uptake regarding protein and RNA. RNA sample's purity is accepted between (1.7 and 1.9)[28].

Quantitative "real-time" polymerase chain reaction (qRT-PCR):

The primers were selected from RT-PCR submitted in the Table1. The reactions of RT-PCR have been achieved on the basis of procedures of manufacturers (Agilent Tech. Stratagene, U.S.). In addition, the isolated RNA has been reverted in the double-stranded cDNAs using Quanti-Fast SYBR Green PCR Master MixKit (abm Kit) with regard to the reverse transcriptase-polymerase enzyme. Also, reaction's amplification condition is in the following way: 15mins at 42 Celsius, denaturation for 19mins at 95 Celsius, and 40 cycles of amplification, each of them for 3seconds and at denaturation temperature 95Celsius, the annealing temperature at 60º Celsius for Endo-G and AIF, yet 58º Celsius for BAX and BCL-2 of 20s., while the elongation temperature at for 20 seconds at 72 Celsius. Each one of the tests has been achieved in RT-PCR tests; a single sample with no cDNA is utilized for each pair of primers, that contain just RNase free water. Furthermore, the ratio of the expression with the calibrator sample has been estimated: the Ct in next formula: CT (testing) = CT gene of interest (targeted, testing) – CT internal control. Gene s average CT was estimated in every one of the samples (a triplicate for every one of them) and applied for normalizing the expression level with the use of ΔΔ CT approach: threshold cycle (Ct) has been estimated, whereas the relative gene expression has been indicated in the following way: fold change = 2^ (−ΔΔCt) [29].

The colloidal NPs have been specified with the use of a ultraviolet-visible spectrum (Shimadzu UV-Vis1800 spectro-photometer utilizing double beam ultraviolet-visible spectro-photometer (PD-303UV)) for the purpose of detecting the surface SPR related to AuNPs and AgNPs at 25 Celsius. In addition, the structural evolution regarding colloidal NPs has been achieved with the use of XRD [Shimadzu XRD6000, AS (3 k.NOPC)] utilizing Cu-Kα-radiation with wave-length (λ = 00.15418nm) that operate at 30mA and 40 kV, while the Debye-Scherrer formula ($D = k\lambda/\beta\cos\theta$, in which D denotes particle's diameter, k representing a constant = 0.940, λ representing the wave-length of the X-ray source, β representing full width at half maximum (FWHM) also θ representing Bragg angle) is utilized for measuring the average crystallite size. Also, the FESEM type Jeol JSM6460 LV microscope has been applied for studying the microstructure and morphology of colloidal NPs.

Results:

As the colour of the prepared solutions of the metal salts is changed, the formation related to metal NPs which have been prepared with a use of Ar jet approach has been changed, the color of solutions is changing because of the reaction process. The color change provides the initial indication regarding NP's formation throughout the process of mixing in metal salt solutions. The non-metal color of metal particles is because of the SPR, which happens in some metals, like gold and silver because its particle diameter reaches nanometre. Thus, spectral analysis device has been utilized at wave-lengths of the visible light for proving the NP's formation, while the UV-Visible absorption spectra related to colloidal AgNPs as an exposure time function that has been indicated in fig (2a). Increment in absorbance might be indicated in the ultrsviolet-Visible spectrum with regard to Ag NPs at 6mins of exposure time compared to the other time, in which peak area at 439nm to 443nm is increasing with the increase in exposure time.

The formation of AgNPs is evidence via the sharp peak at about 443nm [7], whereas increasing the intensity might be because of the more and more NPs created due to the decrease of silver ions existing in aqueous solutions. Fig (2.b), is showing the UV-Visible absorption spectra regarding colloidal AuNPs as a function of the exposure time. In addition, the highest absorption has been at (520nm-525nm) that indicates the particle size is not more than (20nm). The AuNPs that are prepared in 6mins concentration is showing distinctive behavior, while the absorbance spectrum has been elevated in comparison to the other sample. Furthermore, the results verified the presence of AuNPs with the sphere shape, also in accordance with those acquired in literature with regard to light scattering spectra simulation of AuNPs utilizing Mie theory

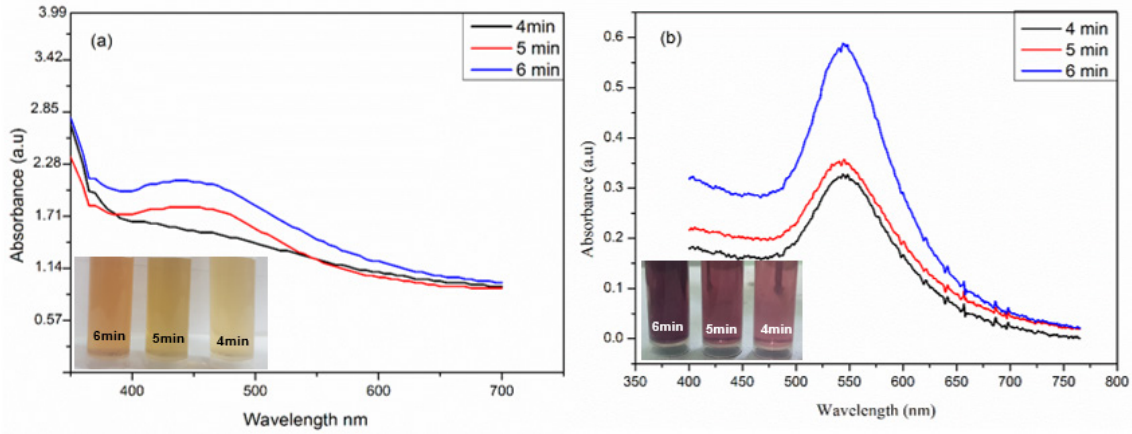

Figure 2. Ultraviolet-visible absorption spectrum of nanoparticles prepared using jet plasma as a function of exposure time: [1] Silver nanoparticles (AgNPs) , [1] Gold nanoparticles (AuNPs)

X-Ray Diffraction (XRD)

Patterns of XRD of the dried Ag NPs which have been synthesized with the use of the Ar jet approach has been altered have shown the Bragg reflection which have been representative of the structures of the fcc of the silver NPs. Fig.3 (a) illustrates spectra of the XRD Ag NPs which have been prepared as an exposure time function, in which the peaks at angles of 38.20 and 44.40, correspond to (111) and (200) planes of Ag, following the matching with the standardized Xray models of the Ag (JCPDS No04-0783). Abovementioned pattern has shown the fact that patterns of the diffraction of any peaks can't be copied into other types of material, indicating the fact of prepared sample's purity and its freedom of any added types of impurity [1]. Increasing the exposure time leads to better crystallization of the X-ray patterns

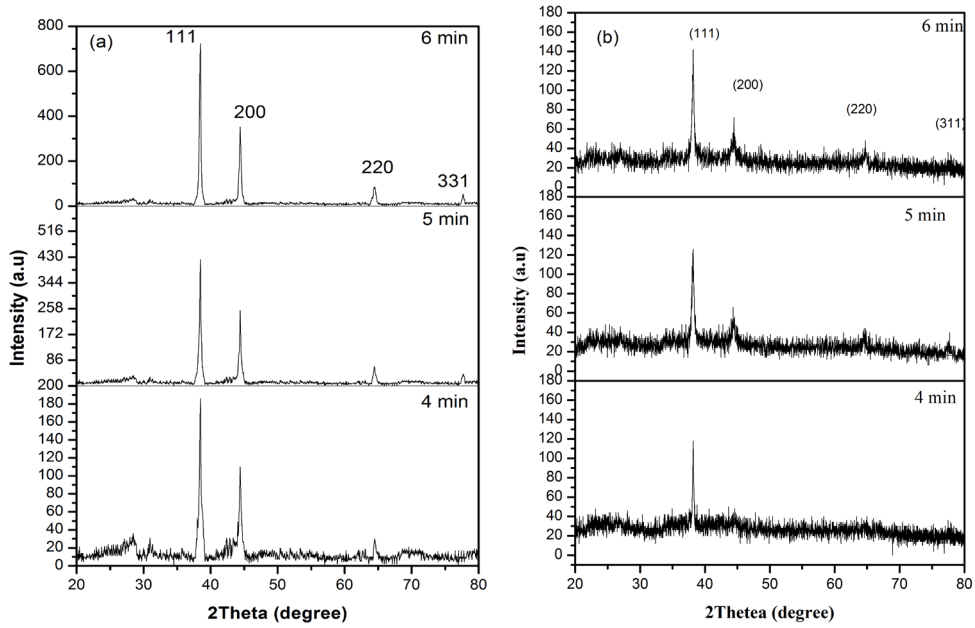

Figure 3. X-ray patterns of NPs which have been prepared with the use of the jet plasma as an exposure time function: [1] Ag NPs ,[1] Au NPs

Field Emission Scanning Electron Microscopy Study

FESEM images (Figure4) demonstrate synthesized Ag NPs and Au NPs morphological characters with the use of plasm jet. Fig. 3a illustrates that well dispersed Ag NPs image, the NPs particle sizes range between 20nm and 41nm with spherical shape. Whereas for Au NPs collide about 26nm-33nm with spherical shapes as can be seen in Fig. 4 .

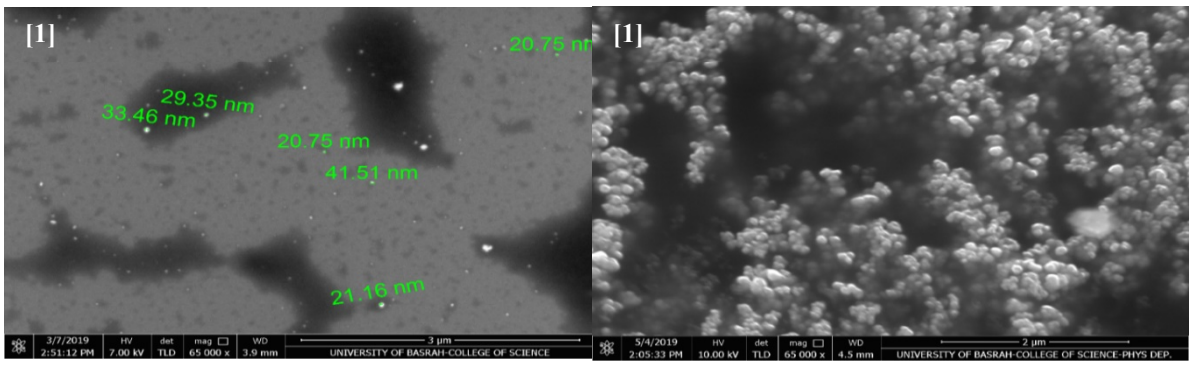

Figure 4. FESEM images of the colloidal nanoparticles prepared using jet plasma: [1]Silver nanoparticles (AgNPs), [1] Gold nanoparticles (AuNPs)

Cytotoxicity Assay:

The in vitro tests of the cytotoxicity have been assessed against the Normal embryonic cell line REF and the digestive system (Skg, HC) cell lines under a variety of the series dilute of the Ag and Au NPs, for the calculation of the effects of the nanoparticles on cancer cell lines. The maximum HC cell line cytotoxicity has been obtained in the case where 100 µg\ml of the Au NP exposure has been 69.60%, whereas 100 µg\ml Au NP exposure has been 69.20% for the SKg cell line. Cytotoxicity of normal cell lines of the REF in the case of the exposure 100 µg\ml Au NPs has been 40.60%, While it gave 46.9% when exposed to a concentration of 100 µg\ml of AgNPs, can be seen in figure5.

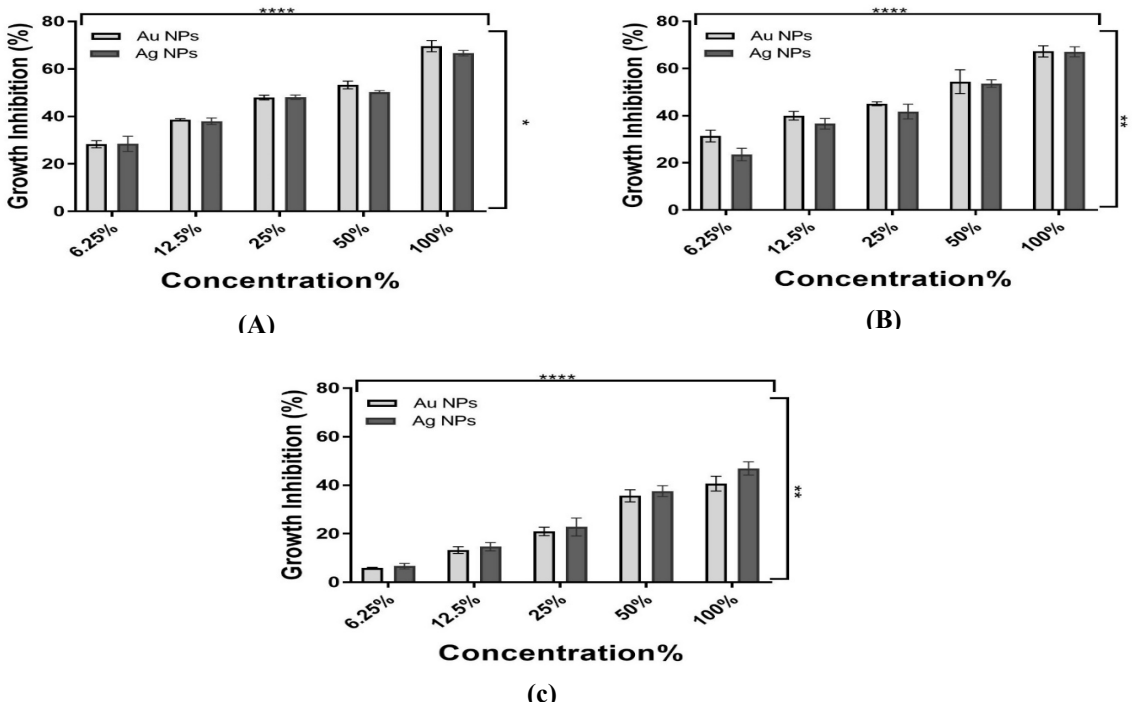

Figure 5. Cytotoxicity assay of AuNPs and AgNPs exposure on (A) HC cell line, (B) SKg cell line and (c) REF cell line

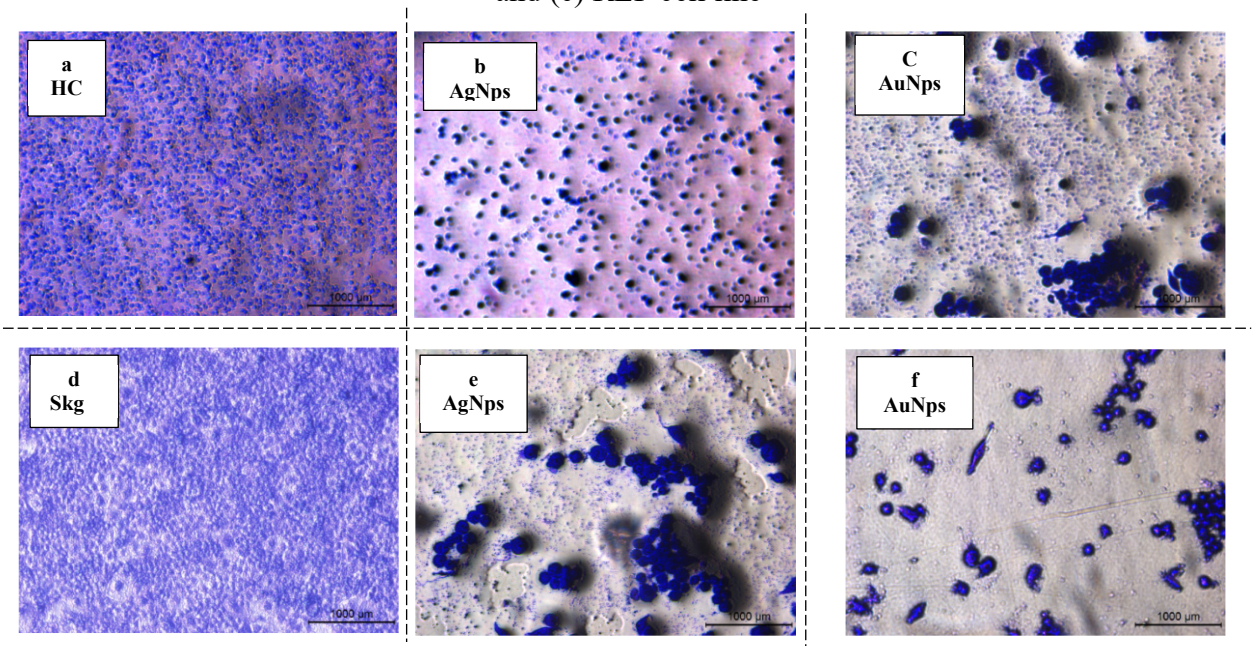

Figure 6. Cancer cell lines which have been stained by the crystal violet stains and examined under the inverted microscope. [1] HC control [1] Ag NPs-treated cell of the HC (c) Au NPs-treated cells of HC [1] Skg control (e) Ag NPs-treated cells of Skg (f) Au NPs-treated cell of Skg

Gene Expression Analysis

AuNPs and AgNPs impacts on the gene expressions for 4 distinct genes Bcl-2 (pro-survival) and BAX (pro-apoptotic), Endo G and AIF (independent path-way) have been assessed in the SKG and the HCAM cell lines. In cell line of HCAM, BAX and Bcl-2 expression have been down-regulated following 48 hours of the incubation time of the Au NPs and Ag NPs, however, EndoG and AIF (Independent pathway) over-expression duration of the Au NPs treated and elevated AIF expression duration of the Ag NPs treated. In cell lines of the SKG, EndoG and AIF (independent path-way) and the over-expression of the BAX in Au NPs however, the Bcl-2 of the down-regulating in the Au NPs

following 48-hour period of the incubation. Ag NPs of the up expression in the AIF (Independent path-way) and the BAX genes however, the downexpression of the Bcl-2 and EndoG following 48-hrs treated. Fig7 shows the impact of optimal Ag NPs and Au NPs which have been produced by the cold plasma on gene.

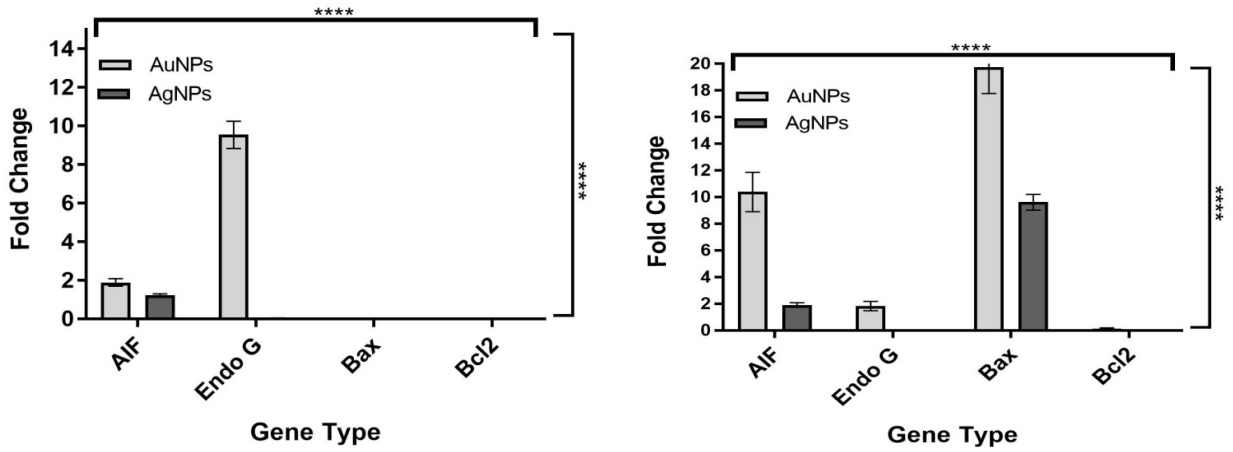

Figure 7. (AIF, Endo G genes) Independent path-way and (Bcl-2 & BAX gene) expression analyses through the relative quantitative real time Polymerase Chain Reaction in the cell line of the (1) HC and (2) SK-GT-4, (AIF, Endo G genes) Independent path-way and (Bcl-2 & BAX genes) expression analyses by the relative quantitative real time

Discussion:

The measurements of the XRD have shown a distinctive pattern for prepared samples. The exposure pattern for 6min time has been more sufficient compare to other sample types. Sherer formula [1] has been utilized for the calculation of the size of the particles. It has been discovered that the optimal size has been for 6min that is 23nm whereas 32nm, 37 nm for respectively 5min, and 4min exposure time. Fig. 3b shows patterns of the XRD of dried particles of Au which have been produced with the use of Jet Plasma as plasma system exposure time. The XRD pattern test results have shown a pattern of the diffraction from the Au NP with an fcc structure of the crystalline. The XRD 2θ peak is 38.18º and 44.44º. It may be traced to 111&200 levels of the crystalline, without any other peak which may result from the impurities. XRD pattern vertices have been centred surrounding the face in the gold because of cubic structure (fcc). The diffraction patterns of the XRD of the Au NPs are corresponding to standard gold JCPDS (file00-004-0784). (111) peak intensity at a diffraction of 38.18 degrees has been considerably stronger compared to (200) peak at 44.44 degrees for presence of the ubiquitous samples at 5 minutes, and 6 minutes. It has been discovered that for the sample which has been produced at 6 minutes include 3 peak values that may result from the 2θ which equals 38.10°, 44.40º, and 66.40º, for (111),(200), as well as (220). The mean value of the Au NPs volume has been computed with the use of the Debye-Scherer equation through the determination of strongest width of the peak. The crystals size for 6min has been 18nm whereas 27nm, 32 nm for 5min and 4min time of exposure. The rustles have shown that the size of the crystal for the collide Ag and Au NPs have been dependent upon the plasma system time of exposure.

FESEM images NPs particle sizes that have been obtained with the use of the images of the microscopic electron microscopy has been nearly equal to that which has been produced by the measurements of the XRD. It has been stated that metallic NPs shapes affects their electronic and optical characteristics.

This study aimed to investigate the involvement of caspase-independent way of apoptosis through treatmen by AuNPs and AgNPs. . The gold and silver nanoparticles showed potent cytotoxicity against HC and SK-GT-4 cancer cells. The biosynthesized nanoparticles showed a direct dose-response relationship, and the cytotoxicity was increased by the increasing concentrations of metal

nanoparticles. The IC50 values of AuNPs and AgNPs were found at 100 μg/ml, respectively which showed significant cytotoxicity in HC and SK-GT-4 cells for 48 hrs. of exposures.

The biosynthesized AuNPs induced over 60 % cell death in HC and SK-GT at the highest concentration of 100 μg/ml. The inhibitory concentration of gold nanoparticles was calculated to be 100 μg/ml, However, the silver nanoparticles have less toxicity against HC and SK-GT-4 cells compared with gold nanoparticles. Recently, Vasanth et al. (2014) proposed the MCF-7 cells treated with silver nanoparticles affected the percentage of cell viability at different ranges of concentrations[30]. The AgNPs show 90 % cell death at 250 μg/ml. The treated cancer cells underwent membrane blebbing, morphological changes and eventually involved in apoptosis. Also, the GNPs treated MDA-MB-231 cells showed slightly higher cytotoxic effects than the silver nanoparticles[31]. However, both silver and gold nanoparticles showed toxic effects with more than 40 % cell death at 100 mg/ml of nanoparticles[32]. The cytotoxic effect of nanoparticles in DL tumor cells was found at 50 μg/ml and above. The cell viability was considerably decreased by the increasing concentration at 25– 300 μg/ml. The AuNPs and AgNPs have been reported to be of various concentrations between 100–300 and 5–50 μg/ml, against different cell lines such as HeLa cells, Hep-2 cells, and MCF-7 cell line [30, 33, 34]. The observations confirm that the nanoparticles toxicity may vary according to the types of cell lines. Also, the size of the metal nanoparticles is also one of the key factors in cytotoxic activity of cancer model [35]. The cell morphological changes in the treated HC and SK-GT cells are shown in Figure 6. The metal nanoparticle-treated cells clearly showed the apoptotic mechanisms that started through the altered cell membranes.

Quantitative real-time polymerase chain reaction (RT-qPCR) is a novel technique to appropriately identify the different patterns of gene expressions in cancer cell lines. We studied the expressions of pro-apoptotic and pro-survival genes such as BCL2, BAX and AIF and EndoG (caspase-independent). The expressions of BCL2 and BAX, AIF and EndoG have shown significant changes in the gold and silver nanoparticle-treated samples compared with the control ($p< 0.05$).

In the present research, AIF and Endo G (caspase-independent pathway) expression was significantly upregulated in gold and silver nanoparticle-treated samples ($p< 0.0001$) in HC and SK-GT cell line. Those data have shown that the nanoparticles could be as well inducing the mitochondrial apoptosis through a caspase-independent path-way in the cell lines of the digestive system.

Previous studies have demonstrated the ability of gold and silver nanoparticles to induce the programmed cell death of cancer cells by activating the caspases-dependent pathway [34, 36]. The current study relies on the susceptibility of gold and silver nanoparticles to the induced of programmed cell death during the activation of the Caspase-independent pathway.

In the present research, caspases-independent apoptosis involvement has been research with the Ag NPs and Au NPs induced apoptosis in the (HCAM) and the (SK-GT4) cell lines in a time and concentration dependent-way. Those results have been generally coinciding with numerous of the newest reports with the use of a variety of the assays which described the interference with the regulations of the DNA following the Au NPs and Ag NPs exposures [18].

Two main path-ways are leading to the apoptosis. One of them begins by the existence of the cell-surface receptors of the death in the membrane, the other one begins by the mitochondria [37]. Bcl2 protein family plasma members are regulating path-ways of the mitochondria [38]. There are 2 Bcl2 antiapoptotic (i.e. apoptosis inhibition) protein and Bax proapoptosis (i.e. the stimulation of the apoptosis) protein groups belong to such a series of the protein [39]. In the physiologic homeostasis of the tissues, the balance between the cell-apoptosis and the proliferation is of high importance, the disturbances may result in the unregulated proliferation of the cells in that balance[40]. Which may result in the development of the malignant phenotypes. Determining tumor progression and malignant transformations may be carried out via the estimation of the apoptosis and proliferation rates [41].

The results showed an increase in the genetic expression of AIF and EndoG after exposure to both the gold and silver particles for each of the cancer cell lines and gave a significant difference ($p< 0.0001$).

The AIF can be described as mitochondrial protein translating in numerous model systems to the nucleus and the cytosol, and mediating the apoptosis which is caspase-independent [42]. Endo G plays a role in the copy, repair and recombination of the DNA of the mitochondria [23], Translates from the mitochondria to nucleus which is resulted from the oxidative stresses [43]. The mitochondria free Endo G is interacting with the AIF in nucleus and plays a role in *Caenorhabditis elegans* with the apoptosis which is caspase independent [44]. The DNA cannot be decreased by the AIF; the AIF as well as the EndoG could be participating in degrading nuclear DNA [45]. Results have shown that AIF / EndoG levels increased throughout the induced apoptosis of the Au NPs and Ag NPs, and the translocation of the AIF and EndoG declined as a result of the silencing of bNIP3. In other words, the BNIP3 plays a role in caspase-independent apoptotic procedure and is lying up-stream the of AIF / EndoG. The activation of PARP1 results in the generation of the PAR in nucleus which has been released to cytosol and results in placing it with the mitochondria for the purpose of inducing AIF release [46]. Mature AIF has a weakly linked external membrane [47], in which the PAR may be detached [42, 46].
The BCL-2 interacting protein 3, affected throughout the Au NPs and ag NPs, has an impact on the caspase-independent path-ways and it is up-stream of the AIF / EndoG. BAX and BCL-2 silencing results in the prevention of the release of the mitochondrial cyt c to the cytosol and the caspase-dependent apoptosis in the embcyoid differentiation of a body [48].
.R. Mettam, L.B. Adams, How to prepare an electronic version of your article, in: B.S. Jones, R.Z. Smith (Eds.), Introduction to the Electronic Age, E-Publishing Inc., New York, 1999, pp. 281-304.

Conclusion

This study has shown that the Ag NPs and the Au NPs which have been produced by the plasma jet kill HCAM and the SK-GT4 cell types in addition to the Au NPs have a little higher effect. The killing impact discovered throughout the induction of the apoptosis is involved with the caspase independent pathways. In addition to that, the Au NPs induced Endo G up-regulation whereas the Ag NPs did not, and that could be referring to another path-way with the killing effect. Those two NPs have been discovered to have lower toxicity in the normal cells, possibly indicating the selective killing impact, suggesting the use of those lately produced NPs in the treatment of cancer.

References

[1] Q. Abdullah, A. Obaid, and M. Bououdina, Influence of gas carrier on morphological and optical properties of nanostructured In2O3 grown by solid-vapour process. Ceramics International. 44(2018)p. 4699-4703.

[2] R. Andrea, Igaz, N., Gopisetty, M. K., Szerencsés, B., Kovács, D., Papp, C., .& Pfeiffer, Biosynthesized silver and gold nanoparticles are potent antimycotics against opportunistic pathogenic yeasts and dermatophytes. International journal of nanomedicine 13 (2018): 695.

[3] Ali Thamer, N., B.H. Adil, and A. Obaid, Gold Nanoparticles Synthesis Using Environmentally Friendly Approach for Inhibition Human Breast Cancer. International Journal of Nanoscience, (2020) p. 1950040.

[4] Kamat, P.V., Photophysical, photochemical and photocatalytic aspects of metal nanoparticles. 2002, ACS Publications.

[5] Zainal, I.G., A.M. Al-Shammari, and W. Kachi, Characterization of the modified nickel-zinc ferrite nanoparticles coated with APTES by salinization reaction. AIP Conference Proceedings. 1968(2018) 030008.

[6] Adil, B.H., A.M. Al-Shammari, and H.H. Murbat, Breast cancer treatment using cold atmospheric plasma generated by the FE-DBD scheme. Clinical Plasma Medicine, 19-20(2020)p. 100103.

[7] Kachi, W., A.M. Al-Shammari, and I.G. Zainal. Cobalt ferrite nanoparticles: Preparation, characterization and salinized with 3-aminopropyl triethoxysilane. in Energy Procedia. 2019.

[8] Sahoo, G. P., Basu, S., Samanta, S., & Misra, A, Microwave-assisted synthesis of anisotropic gold nanocrystals in polymer matrix and their catalytic activities. Journal of Experimental Nanoscience, 10(2015): p. 690-702.

[9] Fajstavr, D., P. Slepička, and V. Švorčík, LIPSS with gold nanoclusters prepared by combination of heat treatment and KrF exposure. Applied Surface Science, 465(2019)p. 919-928.

[10] Scholl, J.A., A.L. Koh, and J.A. Dionne, Quantum plasmon resonances of individual metallic nanoparticles. Nature, 483(2012) p. 421-427.

[11] Yoon, K. Y., Byeon, J. H., Park, J. H., & Hwang, J., Susceptibility constants of Escherichia coli and Bacillus subtilis to silver and copper nanoparticles. Science of the Total Environment. 373(2007): p. 572-575.

[12] Ávalos, A., Haza, A. I., Mateo, D., & Morales, P., Effects of silver and gold nanoparticles of different sizes in human pulmonary fibroblasts. Toxicology mechanisms and methods. 25(2015): p. 287-295.

[13] Liao, C., Y. Li, and S.C. Tjong, Bactericidal and cytotoxic properties of silver nanoparticles. International journal of molecular sciences. 20(2019): p. 449.

[14] Paino, I. M. M., Marangoni, V. S., de Oliveira, R. D. C. S., Antunes, L. M. G., & Zucolotto, V, Cyto and genotoxicity of gold nanoparticles in human hepatocellular carcinoma and peripheral blood mononuclear cells. Toxicology letters, 2012. 215(2): p. 119-125.

[15] Abdal Dayem, A., Hossain, M. K., Lee, S. B., Kim, K., Saha, S. K., Yang, G. M., ... & Cho, S. G., The role of reactive oxygen species (ROS) in the biological activities of metallic nanoparticles. International journal of molecular sciences, 18(2017): p. 120.

[16] G alluzzi, L., Vitale, I., Aaronson, S. A., Abrams, J. M., Adam, D., Agostinis, P., ... & Turk, B, Molecular mechanisms of cell death: recommendations of the Nomenclature Committee on Cell Death 2018. Cell Death & Differentiation, . 25(2018): p. 486-541.

[17] Eisner, V., M. Picard, and G. Hajnóczky, Mitochondrial dynamics in adaptive and maladaptive cellular stress responses. Nature cell biology. 20(2018): p. 755-765.

[18] Kim, S. and D.Y. Ryu, Silver nanoparticle-induced oxidative stress, genotoxicity and apoptosis in cultured cells and animal tissues. Journal of Applied Toxicology. 33(2013): p. 78-89.

[19] Yuan, Y.-G., Q.-L. Peng, and S. Gurunathan, Silver nanoparticles enhance the apoptotic potential of gemcitabine in human ovarian cancer cells: Combination therapy for effective cancer treatment. International journal of nanomedicine, 12(2017): p. 6487.

[20] Ali, Z., M. Jabir, and A. Al- Shammari, Gold Nanoparticles Inhibiting Proliferation of Human Breast Cancer Cell line. Research journal of biotechnology, 14(2019): p. 79- 82.

[21] Falone, S., M.P. Lisanti, and C. Domenicotti, Oxidative stress and reprogramming of mitochondrial function and dynamics as targets to modulate cancer cell behavior and chemoresistance. Oxidative Medicine and Cellular Longevity, 2019.

[22] Dutta, D., Sahoo, A. K., Chattopadhyay, A., & Ghosh, S. S, Bimetallic silver nanoparticle–gold nanocluster embedded composite nanoparticles for cancer theranostics. Journal of Materials Chemistry B. 4(2016): p. 793-800.

[23] Liu, G., Zou, H., Luo, T., Long, M., Bian, J., Liu, X., ... & Liu, Z, Caspase-dependent and caspase-independent pathways are involved in cadmium-induced apoptosis in primary rat proximal tubular cell culture. PloS one,. 11(2016).

[24] Adil Ban, H., M. Al-Shammri Ahmed, and H. Murbat Hamid, Cold Atmospheric Plasma generated by FE-DBD Scheme cytotoxicity against Breast Cancer cells. In AIP Conference Proceedings .)2019), p. 020033)

[25] Sun, Z., Feng, R., Zhang, L., & Xie, H, CO 2 capture and sequestration by sodium humate and Ca (OH) 2 from carbide slag. Research on Chemical Intermediates, . 44(2018): p. 3613-3627.

[26] Mohammed, M.S., M.F. Al-Taee, and A.M. Al-Shammari, Caspase Dependent and Independent Anti-hematological Malignancy Activity of AMHA1 Attenuated Newcastle Disease Virus. International Journal of Molecular and Cellular Medicine, . 8(2019): p. 211.

[27] Krishnamurthy, J., Ramsey, M. R., Ligon, K. L., Torrice, C., Koh, A., Bonner-Weir, S., & Sharpless, N. E, p16 INK4a induces an age-dependent decline in islet regenerative potential. Nature, 443(2006): p. 453-457.

[28] Russell, D.W. and J. Sambrook, Molecular cloning: a laboratory manual. Vol. 1. 2001: Cold Spring Harbor Laboratory Cold Spring Harbor, NY.

[29] Livak, K.J. and T.D. Schmittgen, Analysis of relative gene expression data using real-time quantitative PCR and the 2− ΔΔCT method. methods. 25(2001): p. 402-408.

[30] V asanth, K., Ilango, K., MohanKumar, R., Agrawal, A., & Dubey, G. P., Anticancer activity of Moringa oleifera mediated silver nanoparticles on human cervical carcinoma cells by apoptosis induction. Colloids and surfaces B: Biointerfaces, 117(2014) p. 354-359.

[31] rishnaraj, C., Muthukumaran, P., Ramachandran, R., Balakumaran, M. D., & Kalaichelvan, P. T, Acalypha indica Linn: biogenic synthesis of silver and gold nanoparticles and their cytotoxic effects against MDA-MB-231, human breast cancer cells. Biotechnology Reports. 4(2014) p. 42-49.

[32] G urunathan, S., Han, J. W., Eppakayala, V., Jeyaraj, M., & Kim, J. H.., Cytotoxicity of biologically synthesized silver nanoparticles in MDA-MB-231 human breast cancer cells. BioMed research international, 2013. 2013.

[33] Shankar, S., Jaiswal, L., Aparna, R. S. L., & Prasad, R. G. S. V., Synthesis, characterization, in vitro biocompatibility, and antimicrobial activity of gold, silver and gold silver alloy nanoparticles prepared from Lansium domesticum fruit peel extract. Materials Letters, 2014. 137: p. 75-78.

[34] K uppusamy, P., Ichwan, S. J., Al-Zikri, P. N. H., Suriyah, W. H., Soundharrajan, I., Govindan, N., ... & Yusoff, M. M., In vitro anticancer activity of Au, Ag nanoparticles synthesized using Commelina nudiflora L. aqueous extract against HCT-116 colon cancer cells. Biological trace element research, 2016. 173(2): p. 297-305.

[35] S wamy, M. K., Sudipta, K. M., Jayanta, K., & Balasubramanya, S., The green synthesis, characterization, and evaluation of the biological activities of silver nanoparticles synthesized from Leptadenia reticulata leaf extract. Applied nanoscience, 2015. 5(1): p. 73-81.

[36] Ávalos, A., P. Morales, and A.I. Haza, Manufactured silver and gold nanoparticles-induced apoptosis by caspase-pathway in human cell lines. Toxicological & Environmental Chemistry, 2018. 100(5-7): p. 629-643.

[37] Wang, C. and R.J. Youle, The role of mitochondria in apoptosis. Annual review of genetics, 2009. 43: p. 95-118.

[38] Llambi, F., Moldoveanu, T., Tait, S. W., Bouchier-Hayes, L., Temirov, J., McCormick, L. L., ... & Green, D. R., A unified model of mammalian BCL-2 protein family interactions at the mitochondria. Molecular cell, 2011. 44(4): p. 517-531.

[39] Hatok, J. and P. Racay, Bcl-2 family proteins: master regulators of cell survival. Biomolecular concepts, 2016. 7(4): p. 259-270.

[40] Jan, R., Understanding apoptosis and apoptotic pathways targeted cancer therapeutics. Advanced pharmaceutical bulletin, 2019. 9(2): p. 205.

[41] Enane, F.O., Y. Saunthararajah, and M. Korc, Differentiation therapy and the mechanisms that terminate cancer cell proliferation without harming normal cells. Cell death & disease, 2018. 9(9): p. 1-15.

[42] Dawson, T.M. and V.L. Dawson, Excitotoxic Programmed Cell Death Involves Caspase-Independent Mechanisms, in Acute Neuronal Injury. 2018, Springer. p. 3-17.

[43] FFam, H. K., Choi, K., Fougner, L., Lim, C. J., & Boerkoel, C. F., Reactive oxygen species stress increases accumulation of tyrosyl-DNA phsosphodiesterase 1 within mitochondria. Scientific reports, 2018. 8(1): p. 1-14.

[44] Wiehe, R. S., Gole, B., Chatre, L., Walther, P., Calzia, E., Palmer, A., ... & Wiesmüller, L.., Correction: Endonuclease G promotes mitochondrial genome cleavage and replication. Oncotarget, 2018. 9(45): p. 27908.

[45] Yang, S., Zhao, X., Xu, H., Chen, F., Xu, Y., Li, Z., ... & Ye, J., AKT2 blocks nucleus translocation of apoptosis-inducing factor (AIF) and endonuclease G (EndoG) while promoting caspase activation during cardiac ischemia. International journal of molecular sciences, 2017. 18(3): p. 565.

[46] C Yang, S., Zhao, X., Xu, H., Chen, F., Xu, Y., Li, Z., ... & Ye, J.., Poly (adenosine diphosphate-ribose) polymerase as therapeutic target: lessons learned from its inhibitors. Oncotarget, 2017. 8(30): p. 50221.

[47] Bano, D. and J.H. Prehn, Apoptosis-inducing factor (AIF) in physiology and disease: the tale of a repented natural born killer. EBioMedicine, 2018. 30: p. 29-37.

[48] Li, Y., Zhang, X., Yang, J., Zhang, Y., Zhu, D., Zhang, L., ... & Zhou, J., Methylation of BNIP3 in pancreatic cancer inhibits the induction of mitochondrial-mediated tumor cell apoptosis. Oncotarget, 2017. 8(38): p. 63208.